Numerical investigation of a novel tubular dew-point evaporative cooler

Fangrui Gao [1,2], Kyaw Thu[3], Sibao Wang [1,2,*], Fangyuan Zhao [1], Jie Lin [4,*], Kaiyao Wu [1]

[1] *College of Mechanical and Vehicle Engineering, Chongqing University, Chongqing 400044, China*

[2] *State Key Laboratory of Mechanical Transmission, Chongqing University, Chongqing 400044, China*

[3] *Department of Advanced Environmental Science and Engineering, Faculty of Engineering Sciences, Kyushu University, Kasuga-koen 6-1, Kasuga-city, Fukuoka, 816-8580, Japan*

[4] *Department of Chemical Engineering, Electrochemical Innovation Lab, University College London, Torrington Place, London, WC1E 7JE, UK*

[*]Corresponding Author

Email: wangsibaocqu@cqu.edu.cn (Sibao Wang)

jie.lin@ucl.ac.uk (Jie Lin)

Abstract

Dew-point evaporative cooling can efficiently bring down the air temperature to near dew point through water evaporation. Most dew-point evaporative coolers employing conventional plate type configurations have approached their limit and leveled off. To further improve the performance of dew-point evaporative cooling, a novel counter-flow tubular architecture is proposed in this paper. Based on the momentum, energy and mass balances, a rotating axisymmetric mathematical model is established for the new cooler. The heat and mass transfer process in the cooler is analyzed and compared with that of a conventional plate-type cooler. The cooling intensity, evaporation intensity and convective heat and mass transfer coefficient are discussed to elucidate the advanced cooling behavior of a tubular cooler. The results show that: (1) for ambient air with 30.0–38.0 ℃ temperature and 12.0–20.0 g/kg humidity, the product air temperature of a tube-type dew-point evaporative cooler is 1.6–3.0 ℃lower than that of a plate-type, and the dew-point effectiveness is 0.18 higher;

(2) the working air of the tubular cooler reaches humidity saturation at 0.05 m after entering the wet channel, which is significantly shorter than the plate structure by 0.25 m; (3) in the tubular wet channel, the channel length that achieves active cooling is longer than that of a plate-type cooler, and its convective heat and mass transfer coefficient are above 150 W/(m^2·K) and 0.04 m/s respectively, i.e., 30 W/(m^2·K) higher and 2.7 times to the plate-type cooler.

Keyword: Dew-point evaporative cooling, heat and mass exchanger, advanced evaporative cooler, energy efficiency

Nomenclature

A	area (m^2)
C	specific heat at constant pressure (kJ/(kg · K))
D_{va}	diff usion coefficient (m^2/s)
h_{fg}	latent heat evaporation (kJ/kg)
r_1	internal radius (mm)
r_2	external radius (mm)
k	thermal conductivity (W/(m · K))
L	channel length (m)
P	pressure (Pa)
ra	working air ratio
t	centigrade temperature (℃)
T	thermodynamic temperature (K)
v	Velocity(m/s)
$\dot{m}$	mass flow rate (kg/s)
$\dot{V}$	volumetric flow rate (m^3/s)
$\dot{Q}$	cooling capacity (W)
$\dot{W}$	water evaporation rate (kg/s)
q	cooling intensity (W/m^3)
q_m	evaporation intensity (kg/(m^3·s))
$\bar{h}$	convective heat transfer coefficient (W/(m^2·K)
$\bar{h}_m$	convective mass transfer coefficient (m/s)
Re	Reynolds number

Greek symbols

δ	thickness (mm)
ε	cooling eff ectiveness
μ	dynamic viscosity (Pa·s)
ρ	density (kg/m^3)
ω	humidity ratio (kg/kg)

Subscripts

0	initial state
a	air
d	dry channel
w	wet channel
dp	dew point
in	inlet
out	outlet
f	water film
s	product
pl	plate
sa	saturation
v	water vapor
r	r-direction
z	z-direction

1.Introduction

Ever since Paris Agreement was proposed and became effective in 2020 [1], the entire world is committed to combat the climate change through introducing energy-saving policies, adopting green-energy technologies and executing sustainable development plans, etc. Conserving electricity is an important mission as current power generation is still dominated by coal plants, which is one of the main causes to worldwide air pollution and carbon emissions [2, 3]. Studies show that conventional mechanical air conditioner takes about 40% of the household electricity consumption in temperate industrialized countries and above 50% in the tropics, and the percentage is much larger in tall buildings [4, 5]. Meanwhile, common refrigerants in conventional air conditioners, such as HFCs, usually have a global warming potential equivalent to hundreds to thousands of times of CO_2 and thus can lead to significant greenhouse effects [6]. Therefore, it is of great importance to develop novel cooling technologies that is energy-efficient and environmentally friendly.

Evaporative cooling technology, as driven by latent heat transfer of water evaporation, provides an ideal solution for many cooling applications. With the advantages of high energy efficiency, great cooling capacity, low manufacturing cost and environmental friendliness, many researchers have been devoted to developing evaporative coolers [7-9]. Evaporative cooling is categorized as direct evaporative cooling and indirect evaporative cooling (IEC). Dew-point evaporative cooler (DPEC), as a novel IEC technology proposed by Valeriy Maisotsenko in 1976 [10, 11], can cool the air towards its dew-point temperature with a constant air absolute humidity [12]. DPEC can be further classified into cross-flow and counter-flow according to their flow patterns. Cross-flow DPEC normally obtain 0.55–0.85 dew-point effectiveness with compact structure and low energy consumption, while counter-flow DPEC have dew-point effectiveness above 0.90 at the expense of the higher flow resistance [13].

Recent breakthroughs in DPEC technology have attracted lots of attentions from different research groups. Many studies have been carried out on the cooler design, material development, mathematical modeling, parameter optimization, and operational strategy. To better retain surface wetness and improved heat transfer effectiveness of DPEC, investigations on the water supply, wet channel material and heat and mass transfer medium have been conducted. Al-Zubaydi et al. [14] investigated the water spray configuration on IEC and revealed that the mixed internal and external sprays performed best with the maximum COP of 19.2. Xu et al. [15, 16]

studied different types of wick materials and methods for supplying water in the wet channels. Their results showed that the diffusion and evaporation ability of most textile fabrics are much better than the kraft paper. Furthermore, Xu tested the cooling performance of a dedicated cooler with the Coolmax® fiber pasted on wet channel wall. Under the standard test condition (i.e., dry-bulb temperature of 37.8 ℃ and wet-bulb temperature of 21.1 ℃), the wet-bulb effectiveness and dew-point effectiveness were 1.14 and 0.75, respectively, and the COP reached 52.5 at a working air ratio of 0.36. Liu et al. [17] optimized the flow arrangements of the air and water, the increase of wet-bulb effectiveness and COP were 29% and 35% compared with commercial DPEC. Pervin et al. [18] experimentally compared five new natural porous materials under hot and dry climate. When the inlet air velocities lay in 0.1–1.2 m/s, eucalyptus fibers (EF) and ceramic pipes were the two best materials with cooling effectiveness in the ranges of 0.33–0.72 and 0.26–0.68, and cooling capacity spanning 0.13–0.71 kW and 0.12–0.55 kW. Zhao et al. [19] tested different materials for air channels. They concluded that wick pasted on metal, for example, sintered wick and cooper, is the most suitable material structure. The thermal conductivity and porosity of heat and mass transfer medium materials have negligible impact on the heat and mass transfer process.

Many scholars also analyzed the cooling performance of DPEC under different configurations. Wan et al. [20] investigated the influence of the flow configurations of water and supply air. Their result showed that the configuration with supply air and water film flow conversely had better performance on product air temperature and cooling effectiveness, in contrast to a co-flowing pattern. Min et al. [21] compared counter-flow and cross-flow DPEC with the same size and working conditions, and the channel gap was optimized to be 2–4 mm for both configurations. It was found that counter-flow cooler had 2%–15% better performance on condensation ratio than cross-flow cooler. Operational conditions, number of transfer units, and height to length ratio of the two configurations were also discussed. Zheng et al. [22] studied vapor condensation under hot and humid condition in a cross-flow cooler. It was found that, under full condensation state, the maximum latent heat transfer was 3.90 kW. Baakeem et al. [23] explored the feasibility of a counter-flow DPEC in eight Arab Gulf cities, with the highest relative humidity to be 73% in Jeddah, and validated with the research of Riangvilaikul and Kuma [24, 25]. Yang et al. [26] analyzed the cooling performance of different DPEC. It was found that the cooler with parallel inlet pipes could adapt to humid climates and had a good feasibility, with energy saving rates of 49% and 19% in

Urumqi and Changsha, respectively.

Apart from the experimental work, a few modeling efforts have been established for DPEC. Chun et al. [27] established a thermodynamic model for a dew-point cooling system. It was found that the cooling capacity and COP of the system were negatively correlated. Golizadeh et al. [28] proposed an optimization method for a counter-flow DPEC based on digital twins. Results showed that the surface area and COP of the optimized cooler can be increased by 24% and 73%, respectively. Jafarian et al. [29] used the neural network to predict the cooling effect of a counter-flow DPEC with high accuracy and fast response, and then optimized the cooler based on the prediction model. The optimum result showed that the COP was reduced by 3%, while the overall specific area was increased by 16% in hot climate. Lin et al. [30] proposed a robust optimization framework based on dimensional analysis, regression analysis and multi-to-single-objective optimization. Their optimization results showed that the suggested channel length and ratio of working to supply air are 0.50 m and 0.40 respectively, and the COP can be improved by 36%–92%. Shahram and Maryam [31] numerically investigated three configurations of solar desiccant cooling (SDCS) integrated with DPEC. The best performance was obtained when SDCS used two M-Cycle coolers, with the average COP at 0.728 and product air temperature at 16.1 ℃. Pandelidis et al. [32, 33] simulated eight types of DPEC and analyzed a novel water desalination system based on a modular counter-flow DPEC. A mathematical model was also created and validated. Sohani et al. [34] optimized a counter-flow DPEC to enhance a power generation system. They revealed that the optimized cooler could achieve 9% improvement in the annual net generated power.

It can be summarized that various research projects have been conducted to develop and optimize DPEC through experimental investigations and model predictions. With an emphasis of the flat-plate type heat and mass exchanger, which is easy to model and manufacture, their works have pushed the flat-plate design towards its performance limit and a giant leap is hard to achieve in the future. In flat-plate coolers, the primary convective heat and mass transfer in each channel is one-dimensional and takes place perpendicularly to the air flows. This limits the rate capability of heat and mass transfer in the cooling process. To date, little research has considered heat and mass exchangers beyond a plate-type structure, where the transfer can happen in all transverse directions. A typical idea can refer to the shell and tube heat exchanger, which owns the merits of large heat and mass transfer effectiveness, low electricity consumption, great

compactness, and the ability to induce turbulence [35-38]. Although shell and tube heat exchangers have been popular and widely adopted, little research has ever thought of applying a similar structure to the DPEC.

Herein we aim to boost the performance of the DPEC through developing and investigating a new possible architecture. Gaining insights from the shell and tube heat exchanger, a tube-type DPEC is judiciously designed. A two-dimensional axisymmetric computational fluid dynamics (CFD) model is established for the cooler, by considering the equations of motion, continuity, and energy and mass balances. The cooling performance and heat and mass transfer rate of the new cooler geometry are quantitatively analyzed and compared with a traditional plate-type cooler. The new tubular cooler demonstrates promising cooling performance in cooling intensity, water evaporation intensity and convective heat transfer coefficient.

2.Design of the tubular cooler architecture

The original DPEC has a flat-plate architecture [11, 15, 26, 27, 30, 32], as shown in Fig. 1(a). It is constructed by stacking alternating dry and wet air channels. The dry and wet channels are partitioned by an impervious layer, and a wick material with good water absorptivity is adhered to the inner surfaces of the wet channels. During operation, there are three air streams involved in the cooler, namely, supply air, product air and working air. The supply air from the ambient flows into the dry channels and is separated into two air streams when it reaches the channel ends. One air stream, the product air, is supplied to the room, and the other portion will enter the wet channels to promote water evaporation on the inner walls and is finally discharged to the outdoor as the working air. With this arrangement, the supply air temperature can eventually be reduced approaching to its dew point.

Based on similar working principles, this paper proposes a novel tubular DPEC. As shown in Fig. 1(b), the tubular DPEC is composed of an inner tube, an outer tube shell and two ferrules at tube ends. The inner pipe acts as a dry channel and the annular space between the inner and outer tubes works as a wet channel. A layer of wick material is wrapped around the outer wall of the inner tube to stimulate the evaporative cooling. The ferrules help to position the inner and outer tubes so that they can stay concentric. During operation, the supply air enters the inner pipe from the left end, and the product air exits from the right. Concurrently, the working air flows in the annular wet channel in the opposite direction to the supply air and leaves from the left end of

the cooler. As shown in Fig. 1 (c), in order to increase the cooling capacity, multiple tubular units can be housed together to form a DPEC system which will be vertically configured, and a number of small holes will be drilled around the outer wall at the inlet of the wet channel, and the outer tube will be installed with a fixed chuck to correctly introduce the water to the location of the small holes. During operation, water will be sprayed from the small holes to the wick material on the inner wall of the wet channel. Under the effect of gravity, the water will flow slowly until it is uniformly distributed to the whole wick, and finally flow out along the drainage ditch at the bottom.

The advantages of the tube-type cooler over the plate-type are rather intuitive. On the one hand, due to the annular architecture of tube-type cooler, it provides larger contact surface area per unit channel length when the channel dimensions (diameter) are similar to those (width and height) of a plate-type cooler. Hence, the heat and mass transfer in the air channels are expected to be more effective to achieve better cooling performance. On the other hand, the heat transfer in the tube-type cooler takes place in all radial directions, so a single wet channel is sufficient to cool a dry channel, whereas the heat transfer in a plate-type cooler only happens in a single direction (along the channel height), which consequently requires two adjacent wet channels for each dry channel. This simplifies the manufacturing and assembly of a tube-type cooler.

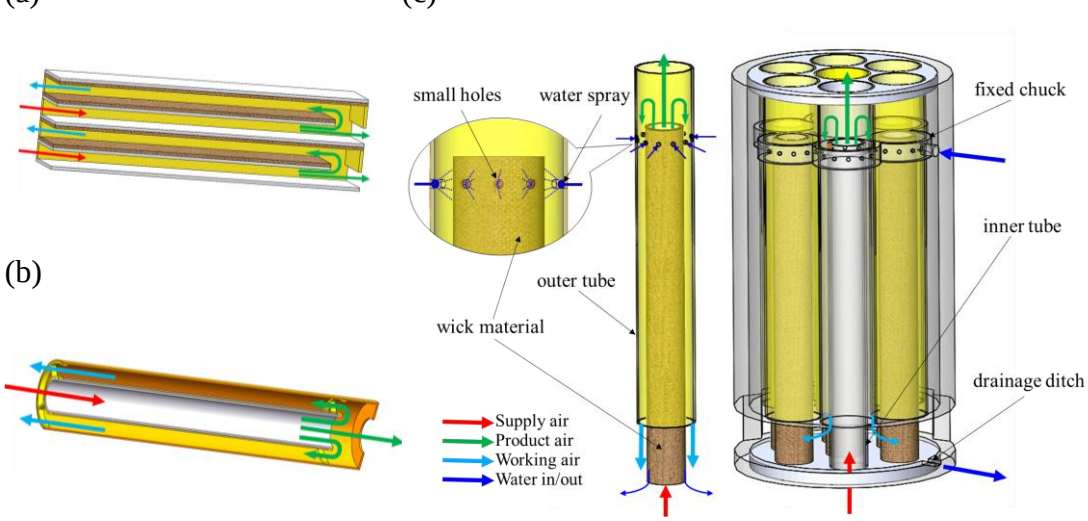

Fig. 1. Counter-flow DPEC structure. (a)Plate structure. (b) Tube structure. (c) DPEC system of tube-type.

3.Modeling and simulation

3.1 Mathematical model

A rotating axisymmetric mathematical model was established to study the performance of the counter-flow tube-type DPEC. As shown in Fig. 2(a) and 2(b), the model geometry of both tube-type and plate-type coolers are composed of four domains. The translucent red and blue areas are dry and wet channels, respectively, between which are the channel wall and water film. For the tube-type cooler, the continuity, momentum balance, energy balance and mass balance of the supply air, working air, channel wall and water film are considered. Before deriving the governing equations of these four parts, the following assumptions are made:

a. The water film is stationary and evenly distributed on the wet channel surfaces, owing to the wettability of the wick material.

b. Variations of the flow field in the circumferential direction of the channels are ignored.

c. The air density is assumed constant in the cooler because of the small changes of air temperature and pressure.

d. The influence of gravity on fluid is not considered.

f. The cooler is well insulated and does not exchange heat with the environment.

The mathematical model of the tubular counter-flow DPEC is shown as follows, and the initial and boundary conditions are summarized in Table 1. The momentum and continuity equations are given in reference [39], and the energy and diffusion equations can be found in reference [40]. However, these four control equations are transformed into a 2D cylindrical coordinates form in this paper.

(a)

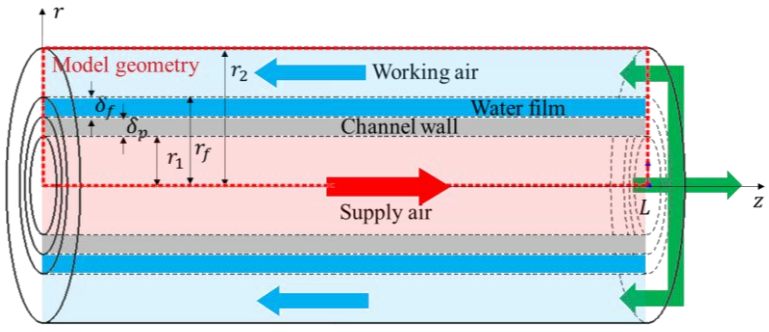

(b)

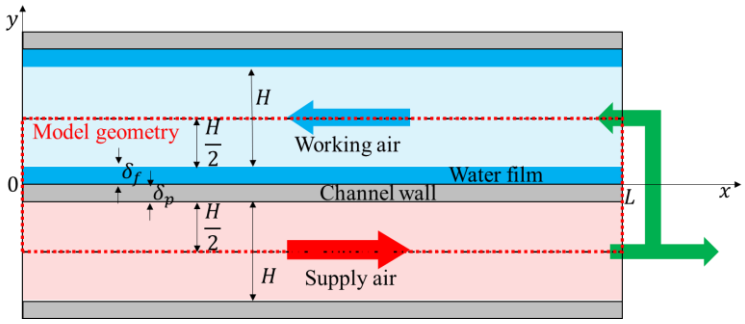

Fig. 2. Model geometry of counter-flow DPEC. (a) Tube-type. (b) Plate-type.

(1) Supply air

Momentum equation:

$$\begin{cases} \rho_a\left(u_{dr}\dfrac{\partial u_{dr}}{\partial r}+u_{dz}\dfrac{\partial u_{dr}}{\partial z}\right)=-\dfrac{\partial P_d}{\partial r}+\mu_a\left[\dfrac{1}{r}\dfrac{\partial}{\partial r}\left(r\dfrac{\partial u_{dr}}{\partial r}\right)+\dfrac{\partial^2 u_{dr}}{\partial z^2}\right] \\ \rho_a\left(u_{dr}\dfrac{\partial u_{dz}}{\partial r}+u_{dz}\dfrac{\partial u_{dz}}{\partial z}\right)=-\dfrac{\partial P_d}{\partial z}+\mu_a\left[\dfrac{1}{r}\dfrac{\partial}{\partial r}\left(r\dfrac{\partial u_{dz}}{\partial r}\right)+\dfrac{\partial^2 u_{dz}}{\partial z^2}\right] \end{cases} \tag{1}$$

where ρ_a is the density of air, u_{dr} and u_{dz} are the velocity of dry air in r direction and z direction respectively, P_d is the pressure of dry air, μ_a is the dynamic viscosity of air.

Continuity equation:

$$\frac{1}{r}\frac{\partial(ru_{dr})}{\partial r}+\frac{\partial u_{dz}}{\partial z}=0 \tag{2}$$

Energy equation:

$$\rho_a C_a\left(u_{dr}\frac{\partial T_d}{\partial r}+u_{dz}\frac{\partial T_d}{\partial z}\right)=k_a\left[\frac{1}{r}\frac{\partial}{\partial r}\left(r\frac{\partial T_d}{\partial r}\right)+\frac{\partial^2 T_d}{\partial z^2}\right] \tag{3}$$

where C_a is the specific heat of air at constant pressure, T_d is the thermodynamic temperature of dry air, k_a is the thermal conductivity of air.

(2) Working air

Momentum equation:

$$\begin{cases} \rho_a\left(u_{wr}\dfrac{\partial u_{wr}}{\partial r}+u_{wz}\dfrac{\partial u_{wr}}{\partial z}\right)=-\dfrac{\partial P_w}{\partial r}+\mu_a\left[\dfrac{1}{r}\dfrac{\partial}{\partial r}\left(r\dfrac{\partial u_{wr}}{\partial r}\right)+\dfrac{\partial^2 u_{wr}}{\partial z^2}\right] \\ \rho_a\left(u_{wr}\dfrac{\partial u_{wz}}{\partial r}+u_{wz}\dfrac{\partial u_{wz}}{\partial z}\right)=-\dfrac{\partial P_w}{\partial z}+\mu_a\left[\dfrac{1}{r}\dfrac{\partial}{\partial r}\left(r\dfrac{\partial u_{wz}}{\partial r}\right)+\dfrac{\partial^2 u_{wz}}{\partial z^2}\right] \end{cases} \tag{4}$$

where u_{wr} and u_{wz} are the velocity of wet air in r direction and z direction respectively, P_w is the pressure of wet air.

Continuity equation:

$$\frac{1}{r}\frac{\partial(ru_{wr})}{\partial r}+\frac{\partial u_{wz}}{\partial z}=0 \tag{5}$$

Energy equation:

$$\rho_a C_a \left(u_{wr}\frac{\partial T_w}{\partial r} + u_{wz}\frac{\partial T_w}{\partial z}\right) = k_a \left[\frac{1}{r}\frac{\partial}{\partial r}\left(r\frac{\partial T_w}{\partial r}\right) + \frac{\partial^2 T_w}{\partial z^2}\right] \quad (6)$$

where T_w is the temperature of wet air.

Diffusion equation:

$$u_{wr}\frac{\partial \rho_v}{\partial r} + u_{wz}\frac{\partial \rho_v}{\partial z} = D_{va}\left[\frac{1}{r}\frac{\partial}{\partial r}\left(r\frac{\partial \rho_v}{\partial r}\right) + \frac{\partial^2 \rho_v}{\partial z^2}\right] \quad (7)$$

where ρ_v is the density of water vapor, D_{va} is the diff usion coefficient of water vapor in the air.

(3) Channel wall

Energy equation:

$$k_{pl}\left[\frac{1}{r}\frac{\partial}{\partial r}\left(r\frac{\partial T_{pl}}{\partial r}\right) + \frac{\partial^2 T_{pl}}{\partial z^2}\right] = 0 \quad (8)$$

where k_{pl} and T_{pl} are the thermal conductivity and thermodynamic temperature of channel wall respectively.

(4) Water film

Energy equation:

$$k_f\left[\frac{1}{r}\frac{\partial}{\partial r}\left(r\frac{\partial T_f}{\partial r}\right) + \frac{\partial^2 T_f}{\partial z^2}\right] = 0 \quad (9)$$

where k_f and T_f are the thermal conductivity and thermodynamic temperature of water film respectively.

Moreover, the necessary thermodynamic and transport properties of moist air can be obtained from the literature [4, 41, 42].

In order to make a comprehensive comparison with a plate-type cooler, the mathematical model of plate-type cooler needs to be established. Here, we transform the transient model established by Lin et al. [43] into a steady-state model, by setting the time derivatives of relevant variables to 0.

Table 1 Initial and boundary conditions.

Supply air	
boundary conditions	Initial conditions
$0 \le z \le L, 0 \le r \le r_1$ $z = 0$: $u_{dz} = u_s, u_{dr} = 0, T_d = T_s$ $z = L$: $u_{wz} = (1 - r_a)u_s, \frac{\partial T_d}{\partial z} = 0$ $r = r_1$: $u_{dz} = 0, u_{dr} = 0, T_d = T_s, k_a\frac{\partial T_d}{\partial r} = k_{pl}\frac{\partial T_{pl}}{\partial r}$ $r = 0$: $\frac{\partial u_{dz}}{\partial r} = 0, \frac{\partial T_d}{\partial r} = 0$	$u_{dr} = 0,$ $u_{dz} = u_s,$ $T_d = T_0$
Working air	
boundary conditions	Initial conditions
$0 \le z \le L, r_1 + \delta_f + \delta_{pl} \le r \le r_2$	$u_{wr} = 0,$

$z = 0$: $P_w = 0, \frac{\partial T_w}{\partial z} = 0, \frac{\partial \rho_v}{\partial z} = 0$	$u_{wz} = 0,$ $T_w = T_0,$ $\rho_v = \rho_{v,sa}(T_0)$
$z = L$: $u_{wz} = -r_a u_s, u_{wr} = 0, T_w = T_d, \rho_v = \rho_{vs}$	
$r = r_1 + \delta_f + \delta_{pl}$: $u_{wz} = 0, u_{wr} = 0,$ $\rho_v = \rho_{v,sa}(T_f),$ $\frac{\partial T_w}{\partial r} + h_{fg} D_{va} \frac{\partial \rho_v}{\partial r} = k_f \frac{\partial T_f}{\partial r}$	
$r = r_2$: $\frac{\partial u_{wz}}{\partial r} = 0, k_a \frac{\partial T_w}{\partial r} = 0, D_{va} \frac{\partial \rho_v}{\partial r} = 0$	

Channel wall	
boundary conditions	Initial conditions
$0 \le z \le L, r_1 \le r \le r_1 + \delta_{pl}$	$T_{pl} = T_0$
$z = L$: $\frac{\partial T_{pl}}{\partial z} = 0$	
$z = 0$: $\frac{\partial T_{pl}}{\partial z} = 0$	
$r = r_1 + \delta_{pl}$: $k_{pl} \frac{\partial T_{pl}}{\partial r} = k_f \frac{\partial T_f}{\partial r}$	

Water film	
boundary conditions	Initial conditions
$0 \le z \le L, r_1 + \delta_{pl} \le r \le r_1 + \delta_{pl} + \delta_f$	$T_f = T_0$
$z = L$: $\frac{\partial T_f}{\partial z} = 0$	
$z = 0$: $\frac{\partial T_f}{\partial z} = 0$	

Note: P_w is a gauge pressure.

3.2 Performance evaluation

Dew-point effectiveness represents the degree of air cooling towards its dew-point temperature by the DPEC, which can be calculated as below

$$\varepsilon_{dp} = \frac{t_{d,in} - t_{d,out}}{t_{d,in} - t_{dp,in}} \tag{10}$$

where $t_{d,in}$ and $t_{d,out}$ are the inlet and outlet temperature of dry air respectively, $t_{dp,in}$ is inlet air dew point temperature.

In addition, the cooling capacity in the dry channel and water evaporation rate in the wet channel of DPEC are expressed as

$$\dot{Q} = \dot{m}_d C_a \left(t_{d,in} - t_{d,out}\right) \tag{11}$$

$$\dot{W} = \dot{V}_w \left(\rho_{v,out} - \rho_{v,in}\right) \tag{12}$$

where $\dot{m}_d$ is the mass flow rate of dry air, $\dot{V}_w$ is the volumetric flow rate of wet air, $\rho_{v,out}$ and $\rho_{v,in}$ are the density of outlet and inlet water vapor in the wet channel respectively.

To analyze the heat transfer rate along the dry and wet channels, the cooling intensity at different channel positions can be evaluated. The cooling intensity represents the cooling capacity per unit volume of the air flow. Hence, for a tube-type cooler, the cooling intensity of dry channel is calculated as

$$q = \frac{d\dot{Q}}{dV} = \frac{\dot{m}_d C_a dt_d}{\pi r_1^2 dz} = \overline{v_d}\rho_a C_a \frac{dt_d}{dz} \tag{13}$$

where $\overline{v_d}$ and t_d are the average cross-section air velocity and temperature in the dry channel respectively.

For a plate-type cooler, the cooling intensity of dry channel is given by

$$q = \frac{d\dot{Q}}{dV} = \frac{\dot{m}_p C_a dt_d}{WHdx} = \overline{v_d}\rho_a C_a \frac{dt_d}{dx} \tag{14}$$

where W and H are the channel width and height of plate-type cooler respectively.

In the wet channel, there are two major forms of heat transfer between the working air flow and the water film, including latent and sensible heat transfer. Latent heat transfer is caused by the water evaporation in the wet channels, and sensible heat transfer is driven by the temperature difference between the working air and the water film, so the cooling intensities of wet channel can be divided into latent heat and sensible heat cooling intensities.

For a tube-type cooler, the latent heat and sensible heat cooling intensities are calculated by the following equations

$$q_L = h_{fg} q_v \frac{dA_f}{dV} = h_{fg} \frac{D_{va}\partial\rho_v}{\partial r} \cdot \frac{2\pi r_f dz}{\left(\pi r_2^2 - \pi {r_f}^2\right)dz} = \left.\frac{2 r_f h_{fg} D_{va}\partial\rho_v}{\left(r_2^2 - {r_f}^2\right)\partial r}\right|_{r=r_f} \tag{15}$$

$$q_S = q_h \cdot \frac{dA_f}{dV} = \frac{k_a \partial T_w}{\partial r} \cdot \frac{2\pi r_f dz}{\left(\pi r_2^2 - \pi {r_f}^2\right)dz} = \left.\frac{2 r_f k_a \partial T_w}{\left(r_2^2 - {r_f}^2\right)\partial r}\right|_{r=r_f} \tag{16}$$

where h_{fg} is the latent heat of water evaporation, q_v is the water film surface evaporation flux, dA_f and dV is water film surface area and air volume with a small channel length. r_f and r_2 are the water film and wet channel radius respectively, q_h is the sensible heat flux on the surface of water film.

As for a plate-type cooler, the latent heat and sensible heat cooling intensities are calculated as

$$q_L = h_{fg} q_v \cdot \frac{dA_f}{dV} = h_{fg} \cdot \frac{D_{va} \partial \rho_v}{\partial y} \cdot \frac{2Wdz}{WHdz} = \left. \frac{2h_{fg} D_{va} \partial \rho_v}{H \partial y} \right|_{y=y_f} \tag{17}$$

$$q_S = q_h \cdot \frac{dA_f}{dV} = \frac{k_a \partial T_w}{\partial y} \cdot \frac{2Wdz}{WHdz} = \left. \frac{2k_a \partial T_w}{H \partial y} \right|_{y=y_f} \tag{18}$$

where $dA_f = 2Wdz$ because water on both the upper and lower sides of the wet channel can evaporate in the plate-type cooler, and y_f is at the water film surface position.

Since the humidity change in the dry channel can be ignored, the mass transfer rate is only analyzed in the wet channel. The evaporation intensity represents the water evaporation rate per unit volume of the air flow. Consequently, for a tube-type cooler, the evaporation intensity of wet channel is calculated as

$$q_m = \frac{d\dot{W}}{dV} = -\frac{\dot{V}_w d\rho_v}{\left(\pi r_2^2 - \pi {r_f}^2\right) dz} = \frac{\overline{v_w}\left(\pi r_2^2 - \pi {r_f}^2\right) d\rho_v}{\left(\pi r_2^2 - \pi {r_f}^2\right) dz} = \overline{v_w} \frac{d\rho_v}{dz} \tag{19}$$

where $\overline{v_w}$ is the average cross-section air velocity in the wet channel.

For a plate-type cooler, the evaporation intensity of wet channel is given by

$$q_m = \frac{d\dot{W}}{dV} = -\frac{\dot{V}_w}{WH} \frac{d\rho_v}{dx} = \frac{\overline{v_w} WH}{WH} \frac{d\rho_v}{dx} = \overline{v_w} \frac{d\rho_v}{dx} \tag{20}$$

The convective heat and mass transfer coefficients in the wet channel are calculated to further measure the cooling performance of the DPEC system. They are defined as the ratio of the longitudinal heat and mass flux of the water film to the average temperature and humidity difference between the water film and the working air respectively[40].

The convective heat transfer coefficients in the wet channel of tube-type and plate-type coolers are calculated as

tube-type: $$\bar{h} = \left. \frac{k_f \partial T_{pl}}{\left(\overline{t_f} - \overline{t_w}\right) \partial r} \right|_{r=r_f} \tag{21}$$

plate-type: $$\bar{h} = \left. \frac{k_f \partial T_{pl}}{\left(\overline{t_f} - \overline{t_w}\right) \partial y} \right|_{y=y_f} \tag{22}$$

where $\overline{t_f}$ and $\overline{t_w}$ are the average temperature of water film and wet film respectively.

The convective mass transfer coefficients in the wet channel of tube-type and plate-type coolers are calculated as

tube-type: $$\bar{h}_m = \left| \frac{D_{va}\partial\rho_v}{(\overline{\rho_f} - \overline{\rho_w})\partial r} \right|_{r=r_f} \quad (23)$$

plate-type: $$\bar{h}_m = \left| \frac{D_{va}\partial\rho_v}{(\overline{\rho_f} - \overline{\rho_w})\partial y} \right|_{y=y_f} \quad (24)$$

where $\overline{\rho_f}$ and $\overline{\rho_w}$ are the average water vapor density of water film and wet film respectively.

The pressure drop appears as the air flows in the channels, so the maximum pressure drop in DPEC is found to be the pressure difference between the dry channel inlet $P_{d,in}$ and wet channel outlet $P_{w,out}$, expressed as

$$\Delta P = P_{d,in} - P_{w,out} \quad (25)$$

3.3 Simulation and grid test

The mathematical model of the cooler is built in COMSOL Multiphysics software. The partial differential control equations, initial conditions and boundary conditions of the dry channel, wet channel, channel wall and water film domains are defined respectively in the software. The model is numerically solved via the finite element method: (1) the model geometry of the cooler is divided into finite small quadrilateral elements through grid; (2) the partial differential control equation is discretized as polynomial equations through approximate interpolation function; (3) the flow, temperature and concentration fields are solved simultaneously.

As shown in Fig. 3(a) and 3(b), the mesh is evenly distributed along the length of the channel, but the junction between the supply air and the channel wall, as well as the junction between the working air and the water film are refined to improve the accuracy of the model. The difference between tube-type and plate-type coolers is that the physical model of tube-type cooler is revolved around the axis of r=0, while a symmetrical condition is set at the lower boundary of the supply air and the upper boundary of the working air in the plate-type cooler.

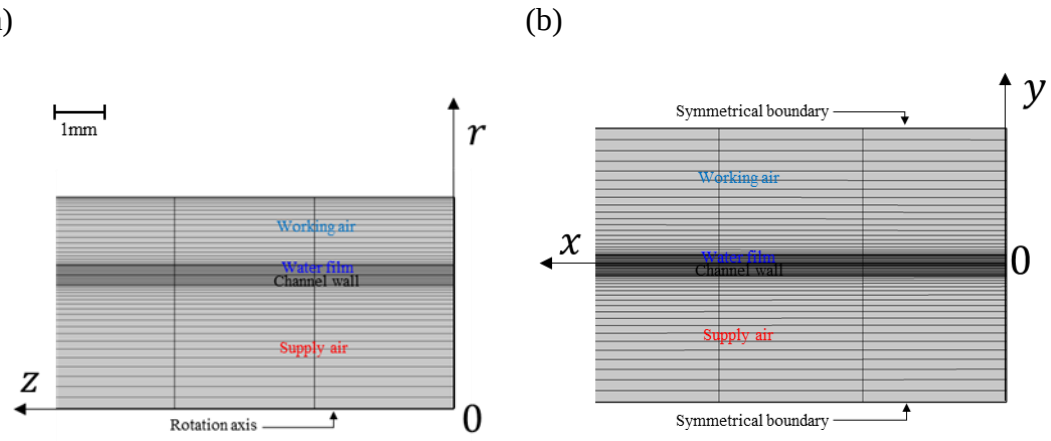

Fig. 3. Grid distribution. (a) Mesh of tube-type cooler. (b) Mesh of plate-type cooler.

The influence of grid size on simulation results is examined, as can be seen in Fig. 4(a). The operating conditions are shown in Table 1 (T_s=30.0 ℃, ω_s=13.3 g/kg, u_s=2.0 m/s, *ra*=0.33).The initial number of cell elements defined in the four domains of the cooler is 100 units along the *z*-axis and 5 units along the *r*-axis. The product air temperature and maximum pressure drop are taken as the indicators. When the number of elements changes from 200×10, 400×20, 600×30 to 800×40 ($z \times r$), the two parameters gradually approach 19.7 ℃and 56.6 Pa. The results show that as the number of elements reaches 400×20, the variation of the simulation results is within 1%. Therefore, considering the changes of simulation processing time and results, a 400 ×20 grid is finally adopted in each domain. The mathematical model of the plate-type cooler is also solved in the same platform, using a 200×20 grid per domain [43].

The simulation results of velocity distribution are shown in Fig. 4(b). It can be seen that the velocity boundary layer hardly changes after 0.1m at the entrance of the dry channel, while it happens in the whole wet channel, which shows that the flow in the tubular DPEC is fully developed. Furthermore, the Reynolds numbers in the dry channel and wet channel are 649 and 80 respectively, and it is indicated that the flow in the tubular DPEC is laminar.

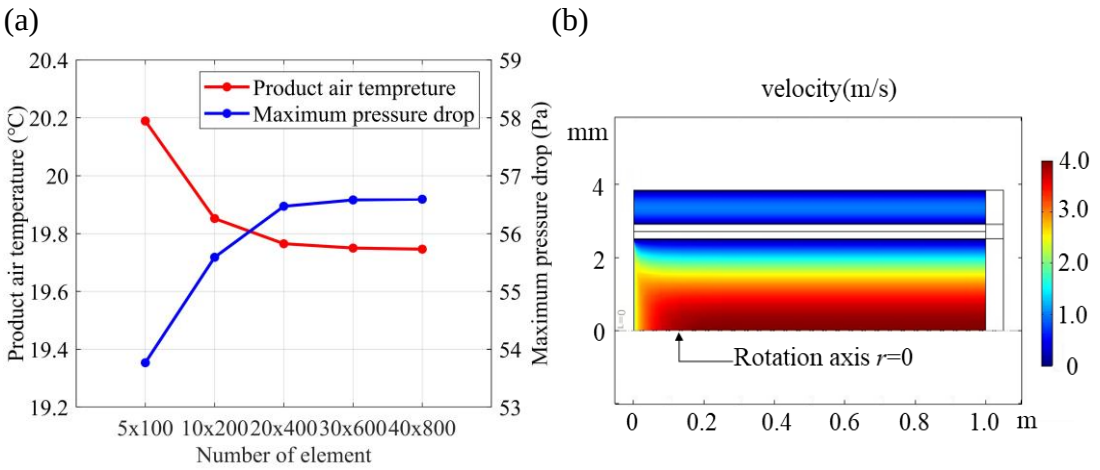

Fig. 4. Simulation results. (a) Influence of grid network. (b) Velocity distribution.

4. Results and discussion

4.1 Model validation

At present, there are little research on DPEC with tubular structure. Even though some studies like Wang et al. [44] and Martinez et al. [45] have studied the IEC and semi-IEC porous ceramic pipes respectively, their devices are different from that is proposed in this work. The present DPEC uses double layers of tubes to form the channel of counter-flow configuration, so each tube unit can work independently and is easy for upscaling. As there is no research on tube-type counter-flow DPEC at present, the accuracy of its model cannot be directly verified. However, considering its similar physics to a plate-type cooler, it is possible to validate the model on a plate-type cooler. With identical model equations, it can be fairly expected that the model can apply to a tube-type cooler. When validating the model, the geometric dimensions of the cooler is set to be consistent with the contrast item, so as to ensure that the hydraulic diameter and Reynolds number are the same.

Table 2 Test conditions for experimental studies.

Studies	Channel length (m)	Channel width (mm)	Channel height (mm)	Normal working to supply air ratio	Reynolds number
Lin et al. [43]	0.6	150	6	0.33	405
Riangvilaikul et al. [24,25]	1.2	80	5	0.33	648
Lee et al. [44]	0.2	9.8	1.5	0.30	179

Fig. 5 compares the results from the plate-type DPEC model established in this paper and the experimental data of Lin et al. [43]. Fig. 5(a) shows their cooler prototype. The relevant parameters of the cooler are shown in Table 2. As seen in Fig. 5(b)-(d), when the working-to-supply air ratio, inlet air temperature, or Reynolds number changes individually, the product air temperature predicted by the model agrees well with the experimental data, and the discrepancy is less than 2%, which exhibits high model accuracy.

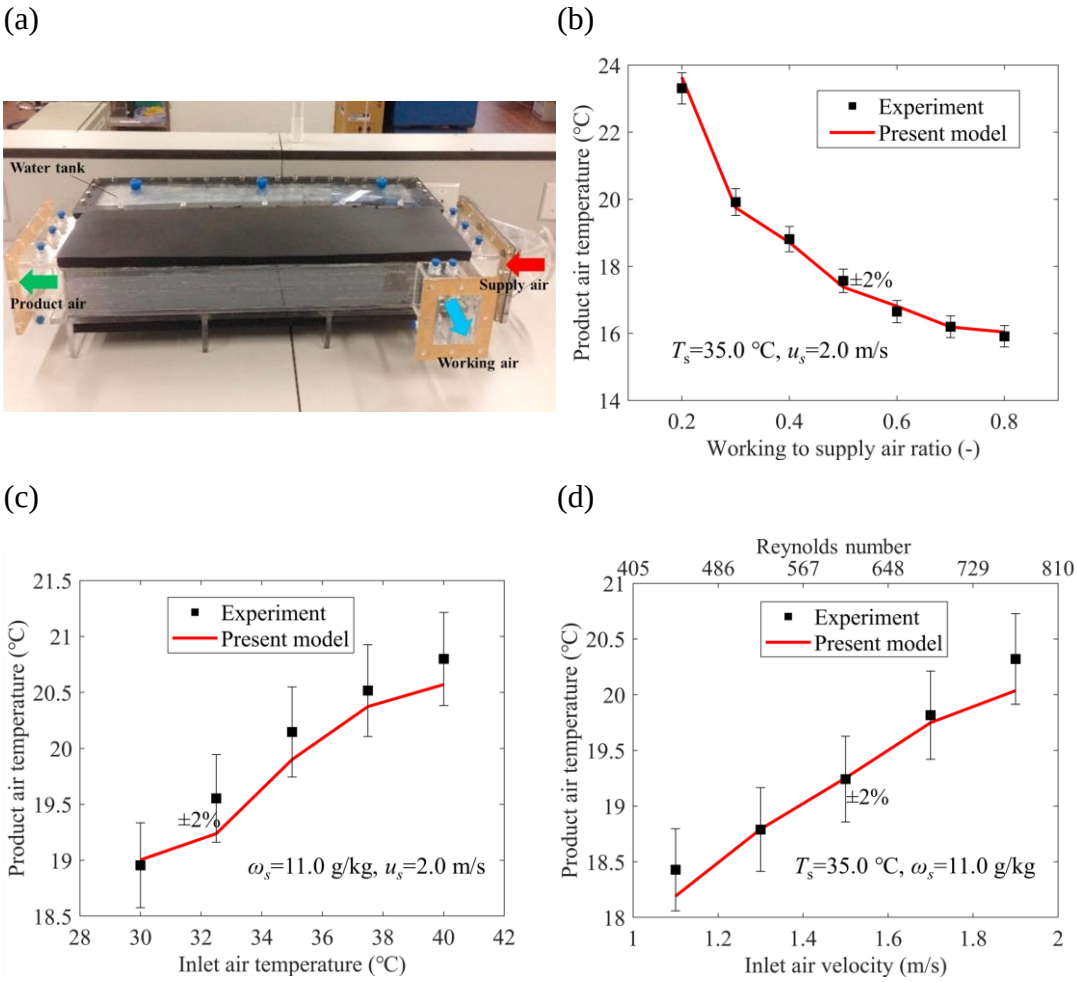

Fig. 5. Model validation of product air temperature with the experiments of Lin et al. [43] under different test conditions. (a) The plate-type cooler of Lin et al. [43]. (b) Working to supply air ratio. (c) Inlet air temperature. (d) Inlet air velocity.

The plate-type cooler model can also be validated with the simulation results and experimental data reported by Riangvilaikul et al. [24, 25], as shown in Fig. 6. The relevant parameters of the counter-flow DPEC are shown in Table 2. Fig. 6(a) shows the product air temperature at different inlet air velocities. The temperature and humidity of the air entering the cooler are 34.0 ℃ and 19.0 g/kg, respectively. The

discrepancy between the mathematical model used in this paper and the experimental data is within 2%, while the discrepancy between the model of Riangvilaikul and the experimental data can be more than 2% at Reynolds number of 607. Keeping the air Reynolds number and the humidity of the supply air at 907 and 20.0 g/kg, respectively, Fig. 6(b) shows the product air temperature at different inlet air temperatures. The maximum discrepancy between the mathematical model used in this paper and the experimental data is still about 2%, when the supply air temperature is less than 40.0 ℃.To sum up, the present model is more accurate than that of Riangvilaikul et al. [24, 25].

(a) (b)

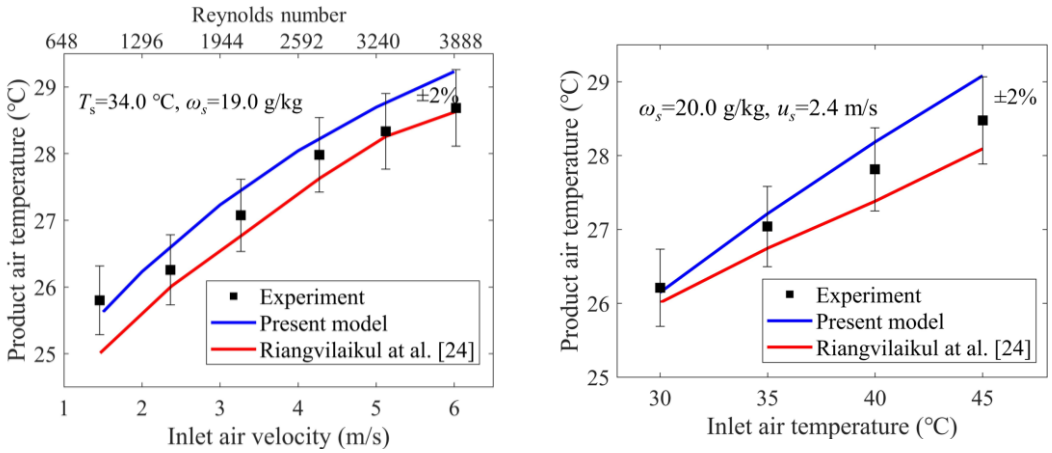

Fig. 6. Model validation of the product air temperature with the data of Riangvilaikul et al. [24, 25] under different test conditions. (a) Inlet air velocity. (b) Inlet air temperature.

In addition, Lee et al. [46] tested a counter-flow DPEC whose channels are finned and their experiments are used to verify the model in this paper. As is seen from Fig.7, the maximum discrepancy between the measured and simulated product air temperature at different relative humidity is less than 6%.

Therefore, the plate-type cooler model used in this paper has been reliably verified by the experimental data and simulation results of three independent studies. Since the model of a tube-type cooler is analogous to that of a plate-type cooler, it can be readily applied to investigate the cooling performance of a tube-type cooler with confidence.

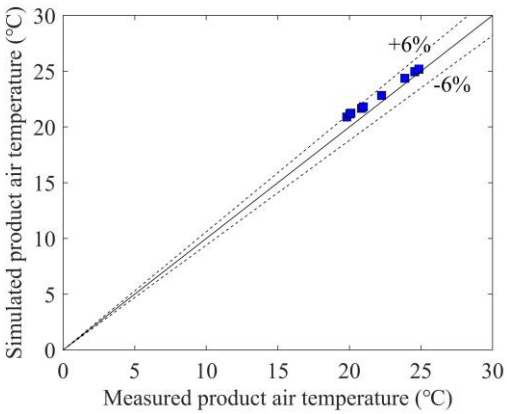

Fig. 7. Model validation by the experiments of Lee et al. [46].

4.2 Temperature and humidity distribution

To gain insights into the performance of the tube-type cooler, it is compared to a plate-type cooler. The nominal structural and working parameters shown in Table 3 are used as input conditions of the simulation model. While selecting the structural parameters, the inner diameter of the tube-type cooler is kept in line with the height of the plate-type cooler, and the outer diameter of tube-type cooler is selected to keep the cross-sectional areas of dry channel and wet channel identical. The width of the plate-type cooler is selected to keep the flow of plate-type and tube-type coolers consistent.

Table 3 Nominal input conditions.

Parameter	Plate-type	Tube-type
Channel length(m)	1	1
Channel width/outer diameter (mm)	4	7.66
Channel height / inner diameter (mm)	5	5
Working to supply air ratio	0.33	0.33
Supply air velocity (m/s)	2.0	2.0
Supply air temperature (℃)	30.0	30.0
Moisture content of supply air (g/kg)	13.3	13.3

The temperature distribution results of plate-type and tube-type coolers are shown in Fig. 8(a), referring to Table 3 for simulation conditions. The temperature difference causes sensible heat flow from the supply air flow to the wall of dry channel, which continuously cools the supply air, The temperature gradient of the supply air is larger in the tube-type cooler, indicating greater cooling intensity. Since the air entering wet channel originates from the dry channel outlet, compared with plate-type cooler, the

tube-type has a lower inlet working air temperature. However, after the working air enters the wet channel of the tube-type cooler, its temperature rises faster and finally exceeds the working temperature of the plate-type cooler. At wet channel outlet, the working air temperature in the tube-type cooler is 1.5 ℃ higher than that in the plate-type. It can be seen from Fig. 8(a) that at the entrance of the wet channel (right end), the initial working temperature is higher than the water film temperature, the sensible heat transfers from the wet channel to the water film. As the working air flows to the left, its temperature gradually decreases to the same temperature as the water film. Compared with the plate-type, this temperature reduction process is much faster for the tube-type cooler, as the working air temperature of plate-type cooler has to pass through a distance of about 0.15 m before reaching equivalent temperature with the water film, while the working air flows less than 0.05 m in the tube-type cooler. After this stage, the working air temperature starts rising and its gradient is almost equal to that of the supply air temperature. For the tube-type cooler, the supply air temperature is 2.0 ℃ higher than that of the working air, while the air temperature difference for the plate-type cooler is 3.5 ℃. From the perspective of heat transfer, it shows that the tube-type cooler achieves more sufficient heat exchange than the plate-type.

In addition, Fig. 8(b) illustrates the humidity distribution of working air for plate-type and tube-type coolers. Because water continues evaporating into the working air, its humidity increases along the flow direction., the working air humidity in the tube-type cooler is greater than that inside the plate-type, indicating that water evaporation in tube-type cooler is more significant. Furthermore, taking the saturation humidity of the working air as a reference, the flow distance required for the working air to saturate in the tube-type cooler is much shorter than that for the plate-type. The air humidity saturation point in the wet channel of plate-type cooler is 0.30 m away from the inlet, while the distance is 0.05 m for tube-type cooler. This results again demonstrates faster water evaporation rate in the tube-type wet channel.

By plotting the temperature and humidity changes of tube-type and plate-type coolers on the psychrometric chart, it is clear that tube-type cooler achieves more efficient cooling. According to Fig. 8(c), when the supply air enters the dry channel, its temperature in both coolers follows the same path. However, at the dry channel outlet, the supply air temperature in the tube-type cooler is reduced to a lower level with the relative humidity of 90%, while the relative humidity of the supply air in the plate-type cooler only reaches 80%. This reveals larger dew-point effectiveness of the tube-type

cooler.

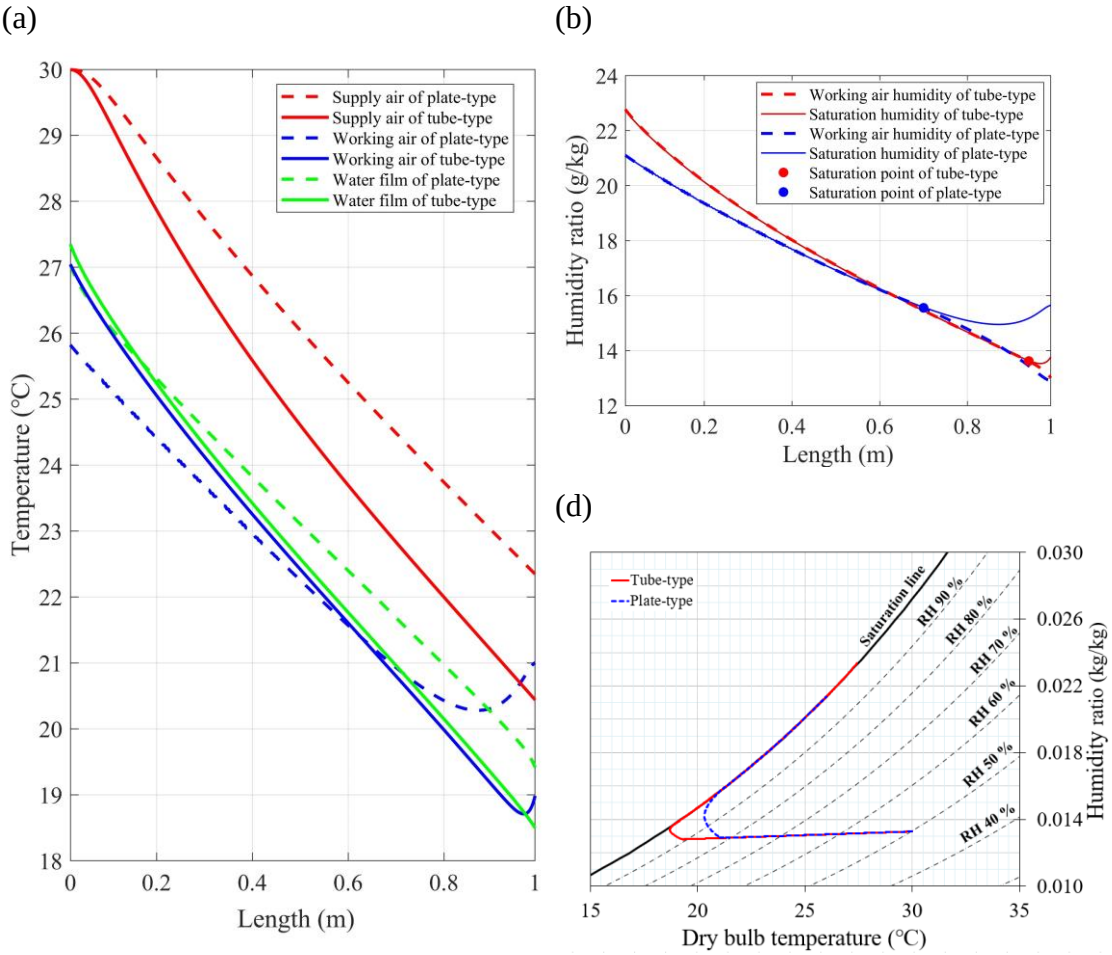

Fig. 8. Temperature and humidity distribution along the channel. (a) Temperature distribution. (b) Humidity distribution in wet channel. (c) Working process on the psychrometric chart.

4.3 Performance comparison and analysis

Table 4 shows the results of product air temperature and dew-point effectiveness. It can be seen that the tube-type cooler has better cooling performance than the plate-type, and the dew-point effectiveness of tube-type cooler is up to 0.86, which is 0.14 higher than the plate-type. Further, air pressure drops of the two coolers can be calculated from the mathematical model. The dry channel pressure drop of tube-type cooler is 6.6 Pa lower than that of the plate-type, but 35.4 Pa higher in the wet channel.

Table 4 Simulation calculation results.

Parameter	Plate-type	Tube-type
Product air temperature (℃)	21.7	20.1
Dew-point effectiveness	0.72	0.86

Dry channel pressure drop (Pa)	52.2	45.6
Wet channel pressure drop (Pa)	20.7	56.1

In order to further verify the advantages of the tube-type cooler, the cooling temperature and dew-point effectiveness of tube-type and plate-type coolers are compared when changing the temperature and humidity of the working environment, and the results can be seen in Fig. 9. When the inlet humidity remains constant at 16.0 g/kg and the inlet temperature changes in the range of 30.0–38.0 ℃, according to Fig. 9(a), the product air temperature of tube-type cooler is 1.6–3.0 ℃ lower than that of the plate-type. The working environment temperature has a less impact on the cooling effect of tube-type cooler, and the product air temperature is stable at 22.0–22.5 ℃. The higher the inlet air temperature, the better the cooling effect of tube-type cooler than that of the plate-type. The dew-point effectiveness is presented in Fig. 9(b). The dew-point effectiveness of the tube-type cooler is about 0.93 while that of the plate-type is around 0.75. When the inlet air temperature stays at 34.0 ℃ and the inlet air humidity spans 12.0–20.0 g/kg, according to Fig. 9(c), the product air temperature of tube-type cooler is 1.8–3.0 ℃ lower than that of the plate-type, and the humidity has a great impact on the cooling effect of both coolers. The lower the inlet air humidity is, the colder the product air of tube-type cooler is than that of the plate-type. The dew-point effectiveness at different inlet air humidity is plotted in Fig. 9(d). The dew-point effectiveness of tube-type cooler varies between 0.88 and 0.96, and that of plate-type cooler varies between 0.70 and 0.78.

(a) (b)

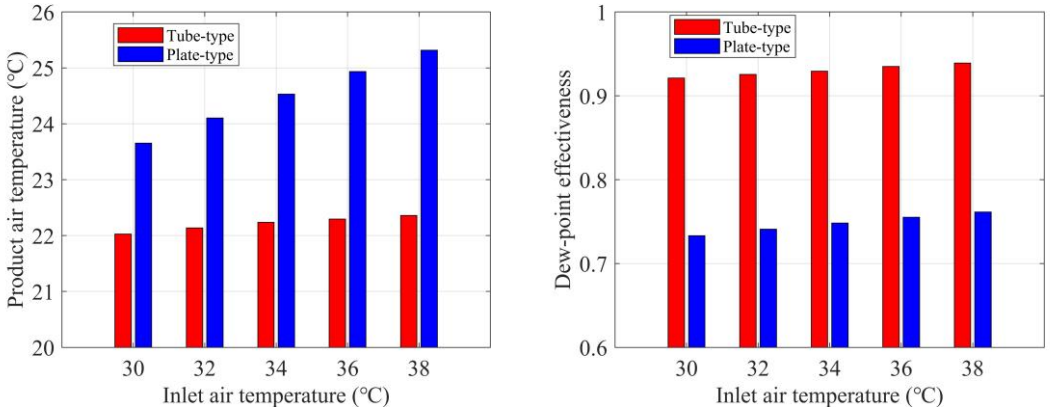

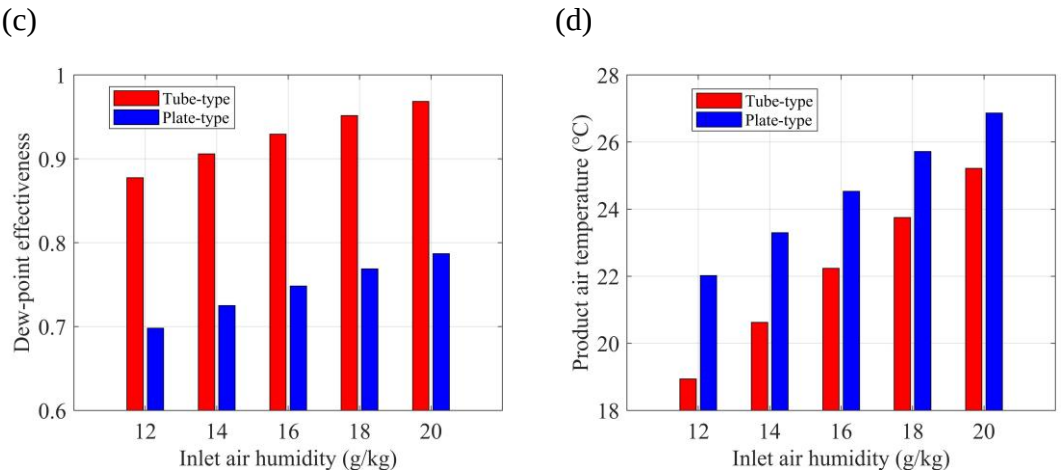

Fig. 9. Performance comparison. (a) Cooling effect under different temperatures. (b) Dew-point effectiveness at different temperatures. (c) Cooling effect under different humidity. (d) Dew-point effectiveness at different humidity.

4.4 Heat transfer along the channel

The cooling intensity (cooling capacity per unit supply air volume) of the tube-type and plate-type coolers along the dry channel are investigated in Fig. 10(a). Regardless of the cooler architecture, the cooling intensity presents similar variations. Along the channel, the cooling intensity is large at the channel entrance, then gradually decreases to a plateau, and finally rises slightly at the dry channel outlet. The large cooling intensity at the channel entrance region is attributed to the large temperature difference between the air stream and channel wall, and more importantly, the developing hydraulic and thermal boundary layers that enhance heat transfer. Similarly, the slight rise of the cooling intensity at the dry channel exit is due to the entry effect in the adjacent wet channel. When comparing the cooling intensity of tube-type and plate-type coolers, it is observed that the cooling intensity of the tube-type cooler is greater than that of the plate-type at all positions of the channel, which accounts for the lower air temperature of tube-type cooler. In addition, the cooling intensity of the tube-type cooler is significantly higher within the first 0.60 m of the channel. This agrees with the temperature distribution in Fig. 8(a), where the supply air temperature gradient of the tube-type cooler is much larger than that of the plate-type in the range of 0–0.60 m. This results in a lower temperature level of the supply air in the tube-type cooler.

According to the breakdown of cooling intensity in Fig. 10(b), the wet-channel heat transfer of the plate-type and tube-type coolers is analyzed. It can be found that the sensible heat cooling intensity of the tube-type cooler is always larger than the plate-type, demonstrating higher convective heat transfer rate. The latent heat cooling

intensity of tube-type cooler is only larger than the plate-type in the latter half of the channel (left) where has greater evaporation, which can be confirmed by the evaporation intensity in Fig. 11(a) of the next section. In the first half of the channel (right), the latent heat cooling intensity of tube-type cooler is slightly lower than that of the plate-type because the working air humidity of the tube-type cooler reaches saturation first, which inhibits the latent heat transfer. Nonetheless, for the tube-type cooler, the area where the latent and sensible heat are parallel occupies almost the entire channel length, while the cooling effect of the plate-type cooler is partially offset by sensible heat owing to its opposite direction to the latent heat transfer in the channel length before 0.12 m. Finally, with the coupled effect of sensible and latent heat transfer, the cooling intensity of tube-type cooler is larger, as shown in Fig. 10(a).

Based on the temperature distribution results in Section 4.3 and above analysis of cooling intensity, the convective heat transfer coefficient is analyzed. As presented in Fig. 10(c), the wet channel can be divided into left and right regions, and their boundary is the position where working air and water film are in thermal equilibrium. Since there is no sensible heat transfer at this location, the convective heat transfer coefficient is calculated to be infinite. It is shown in Fig. 8(a) that the water film temperature is higher than the temperature of working air at a length close to the wet channel outlet, where corresponds to the left area in Figure 9(c), so the sensible heat flows from water film to working air, which is consistent with the latent heat. But near the wet channel entrance, water film is colder than working air, which leads the sensible heat in the right region to be opposite to that in the left region. Therefore, only the latent heat contributes to cooling in the entrance region, while the sensible heat has a negative impact, which leads to the convective heat transfer coefficient of the right region is lower than that in the left in Fig. 10(a). Hence, the evaporative cooling is dominated by the left region, which will well explain why the tube-type cooler has better cooling effect. On the one hand, the convective heat transfer coefficient in the left region of tube-type cooler is above 150 W/(m^2·K), and it is about 100 W/(m^2·K) in the plate-type cooler. On the other hand, the length of the left region of a tube-type cooler is greater than 0.95 m, while the length of the left region of plate-type cooler is only 0.88 m. Both of these merits contribute to the better cooling effectiveness in a tube-type cooler.

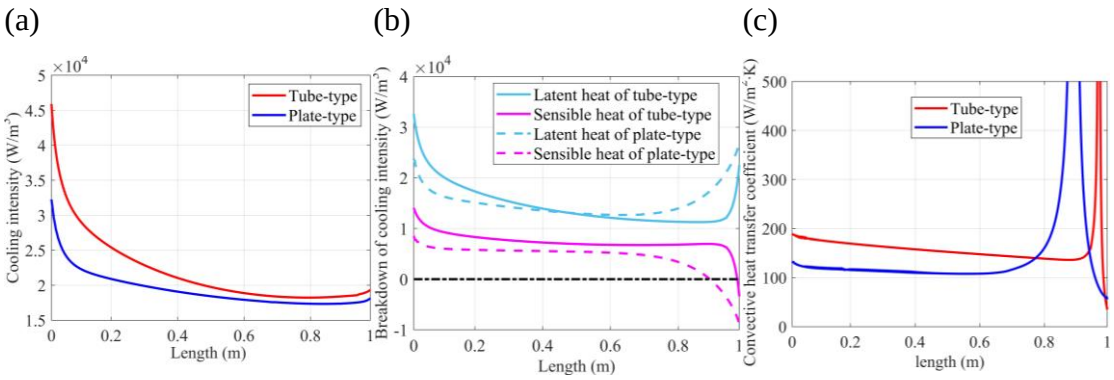

552 **Fig. 10.** Heat transfer along the channels. (a) Cooling intensity in the dry channel. (b)
553 Cooling intensity in the wet channel. (c) Convective heat transfer coefficient.
554

555 ## 4.5 Mass transfer in the wet channel

556 Fig. 11(a) shows the evaporation intensity (water evaporation rate per unit working
557 air volume) along the wet channel. Similar to the cooling intensity of dry channel, the
558 evaporation intensity decreases first at the channel entrance (right) and rises at the
559 channel exit (left). Large water evaporation intensity is obtained when the working air
560 humidity is unsaturated, and it is reduced to a minimum when the working air reaches
561 a saturation point. The flow distance for the evaporation intensity to reach the minimum
562 is 0.30 m in the plate-type cooler, and 0.05 m for the tube-type cooler. which is
563 consistent with the humidity distribution in Fig. 8(b). After the working air humidity
564 saturates, the water evaporation is mainly driven by the rise of working air temperature.
565 When comparing the evaporation intensity in the two cooler types, it is found that it
566 drops faster at the first 0.30 m from the wet channel entrance in the tube-type cooler.
567 However, in the rest channel length of 0.70 m, the evaporation intensity of the tube-
568 type cooler is greater than that of the plate-type, because of its higher water film
569 temperature.

570 Fig. 11(b) shows the convective mass transfer coefficients of the two type coolers.
571 Along the length of wet channel, the convective mass transfer coefficient almost
572 remains stable, and it reaches above 0.04 m/s for the tube-type cooler, while that of the
573 plate type is under 0.02 m/s. In Fig. 11(a), the evaporation intensity of the tube-type
574 cooler does not always dominate the plate-type, but its convection mass transfer
575 coefficient is found to be superior.

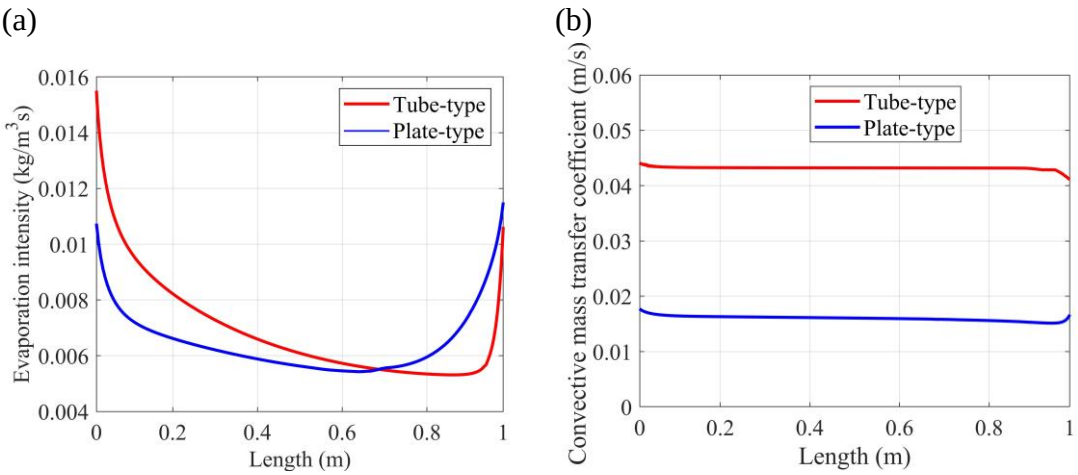

Fig. 11. Mass transfer in the wet channel. (a) evaporation intensity in the wet channel. (b) Convective mass transfer coefficient.

4.6 Influence of working parameters and structural parameters on cooling effect

Now that the tube-type cooler is demonstrated to be a better architecture for evaporative cooling, in order to guide future experiments, the effects of some parameters are studied. The factors affecting cooling performance can be divided into structural parameters (including cross-section radius of inner and outer tubes of the cooler, length of the cooler) and operating parameters (including velocity of working air, the ratio of working to supply air, temperature, and humidity of supply air).

The cooling performance under varying inner radius and outer radius between 1–3 mm and 4–6 mm respectively is investigated in Fig. 12(a) and Fig. 12(b). It is apparent that temperature of product air changes from 18.0 ℃ to 24.0 ℃ with the decrease of both inner and outer radius, the temperature of the product air will decrease. When internal radius is below 2 mm, the product air temperature and dew-point effectiveness are under 20.0 ℃ and over 0.85, respectively. Therefore, in order to deliver lower product air temperature and increase dew-point effectiveness, the inner and outer radius can be appropriately reduced.

The influence of length and radius of the cooler on cooling performance is explicated in Fig. 12(c) and Fig. 12(d). The channel length is extended from 0.50 m to 1.00 m and outer radius is increased from 4 mm to 6 mm (the inner radius is set half of the outer radius). The results show that the product air temperature varies within 19.0–26.0 ℃, and dew-point effectiveness is about 0.85 with outer radius and length set within 4–5 mm and 0.60–1.00 m. Increasing the tube length is more effective than increasing

its radius.

The influence of product air velocity and ratio of working to supply air on the cooling performance is explicated in Fig. 12(e) and 12(f). When the ratio of working to supply air is less than 0.25 and the velocity of product air ranges from 0.5 to 4.5 m/s, the temperature of product air is higher than 24.0 ℃, which is mainly influenced by the ratio of working to supply air. However, when the ratio of working to supply air is greater than 0.25, air velocity dominates the influence on product temperature which ranges from 18.0 ℃ to 24.0 ℃. When the air velocity and the ratio of working to supply air are regulated below 2.0 m/s and over 0.4, the dew-point effectiveness reaches above 0.85, with insignificantly change in the temperature of product air.

Fig. 12(g) and 12(h) show the influence of ambient condition on cooling performance. The temperature of product air gradually rises from 17.0 ℃ to 25.0 ℃, as the temperature and humidity of supply air are regulated within 30.0–40.0 ℃ and 10.0–20.0 g/kg, respectively. The humidity of supply air has a greater impact on the temperature of product air, with dew-point effectiveness keeping above 0.82. The rise of air humidity results in the increase of dew-point temperature, hence deteriorating the cooling effect. When the supply air humidity is below 16.0 g/kg, the product air temperature is lower than 22.0 ℃.

(a)

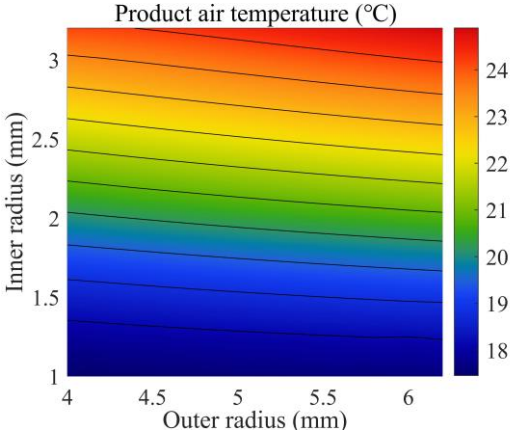

(b)

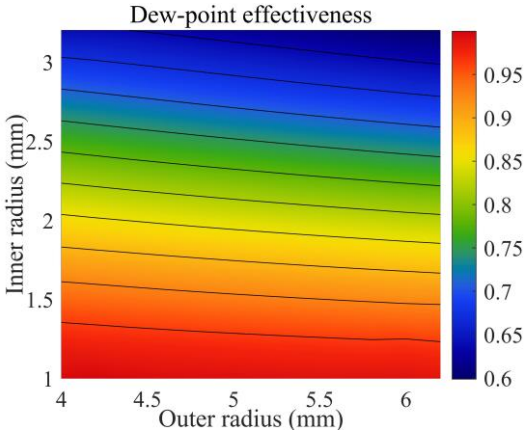

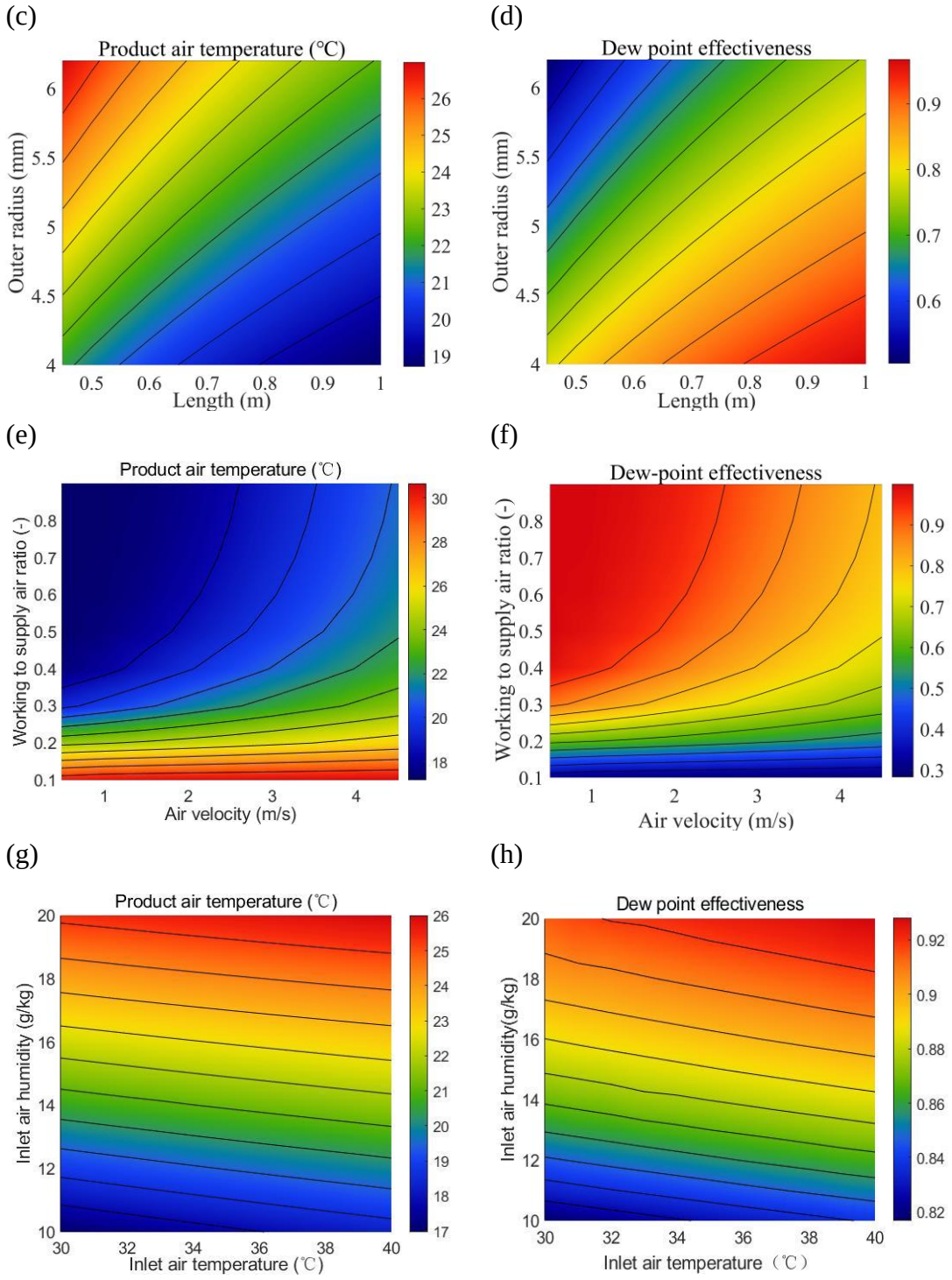

Fig. 12. Influence of parameters. (a) Inner and outer radius on product air temperature. (b) Inner and outer radius on dew-point effectiveness. (c) Radius and length on product air temperature. (d) Radius and length on dew-point effectiveness. (e) Air velocity and ratio of working to supply air on product air temperature. (f) Air velocity and ratio of working to supply air on dew-point effectiveness. (g) Supply air operating parameters on product air temperature. (h) Effect of temperature and humidity on dew-point effectiveness.

5. Conclusions

A counter-flow DPEC with tubular architecture is proposed. A rotating axisymmetric mathematical model based on continuity, momentum, and energy equations along with the performance models is established. The heat and mass transfer process and the influence of working parameters and structural parameters are analyzed. When the ambient temperature changes from 30.0 to 38.0 ℃ or the ambient humidity changes from 12.0 to 20.0 g/kg, the product air temperature of tube-type cooler is 1.6–3.0 ℃ lower than that of traditional plate-type cooler, equivalent to 0.18 higher dew-point effectiveness.

The performance of the DPEC can be expressed in the position of the wet channel air saturation point. When the length of plate-type and tube-type coolers are 1.00 m, the saturation point of them are 0.30 m and 0.05 m away from the wet channel inlet, respectively. The working air of tube-type cooler reaches saturation earlier than that of plate-type cooler, which explains its higher dew point effectiveness.

The evaporation intensity of tube-type is greater than that of plate-type within the last 70% length of the wet channel, and the advantage of tube-type cooler cooling intensity is more obvious. Its cooling intensity is greater in the whole channel length, which also intuitively reflects the superior performance of tube-type cooler.

For the tube-type and plate-type coolers, the length where sensible and latent heat simultaneously plays the cooling role accounts for 95% and 88% of the total wet channel length, respectively. The convective heat and mass transfer coefficient of tube-type cooler are above 150 W/(m^2·K) and 0.04 m/s, while that of the plate-type are under 120 W/(m^2·K) and 0.02 m/s. All these results show that the tube-type architecture has better heat and mass transfer performance, demonstrating itself to be a potentially superior design compared to the traditional plate-type architecture.

There is no doubt that the tube-type DPEC has excellent performance, but the numerical model in this paper still has some limitations. For example, the water flow characteristics on the tube surface can be considered as there can be falling film and non-uniform water distribution if the water supply is not precisely controlled. We hope that our future research can improve this numerical model and build an experimental platform for verification.

Acknowledgements

The authors gratefully acknowledge the generous funding from (1) Chongqing Overseas return innovation funding project (cx2021035); (2) Chongqing Talent Program (CQYC2021058965); and (3) Independent project of State Key Laboratory of Mechanical Transmission (SKLMT-ZZKT-2021R04).

References

[1] J. Blau. The Paris Agreement. The Paris Agreement2017.

[2] R. Amit, S. Ashish, J.K. C. A Solution for Power Crisis and Environment Pollution from Electricity Generation - A Study of Sub-tropical Regions. Smart Science. 9 (2021).

[3] Y. Hui, W. Ernst, C.-G. Wina, Z. Shaohui. The potential of industrial electricity savings to reduce air pollution from coal-fired power generation in China. Journal of Cleaner Production. 301 (2021).

[4] J. Lin, K. Thu, T.D. Bui, R.Z. Wang, K.C. Ng, M. Kumja, et al. Unsteady-state analysis of a counter-flow dew point evaporative cooling system. Energy. 113 (2016).

[5] L. Perez-Lombard, J. Ortiz, C. Pout. A review on buildings energy consumption information. Energy and buildings. 40 (2008) 394-8.

[6] B.Hadya, P.U. Sri, S. Akella. Comparative Study of Eco-friendly Refrigerants in a Lower Capacity Air-Conditioning System. Planetary Scientific Research Center Conference Proceedings Volume 18, Bangkok,Thailand, 2012.

[7] T. Kanghao, Q. Yinghong, D. Taiyang, L. Lingling, Z. Lei, W. Junsong. Biochar from waste biomass as hygroscopic filler for pervious concrete to improve evaporative cooling performance. Construction and Building Materials. 287 (2021).

[8] F. Riaz, M.A. Qyyum, A. Bokhari, J.J. Kleme, M. Lee. Design and Energy Analysis of a Solar Desiccant Evaporative Cooling System with Built-In Daily Energy Storage. Energies. 14 (2021) 2429.

[9] C. Ziran, R. Lin, H. Shoudao, Y. Jie. Research on Noise Reduction of 3.6 MW Evaporative Cooling Wind Motor Induced by Electromagnetic and Two-Phase Flow Resonance Based on Stator Optimization. Processes. 9 (2021).

[10] Y. Hongxing, S. Wenchao, C. Yi, M. Yunran. Research development of indirect evaporative cooling technology: An updated review. Renewable and Sustainable Energy Reviews. 145 (2021).

[11] A. Sujatha, P. Karthik, R. Velraj. Experimental study on the direct evaporative air-cooling system with vermicompost material as the water storage medium. Sustainable Cities and Society. (2021).

[12] Glanville, Paul, Kozlov, Aleksandr, Maisotsenko, Valeriy. Dew Point Evaporative Cooling: Technology Review and Fundamentals. Ashrae Transactions. (2011).

[13] X. Zhao, J.M. Li, S.B. Riffat. Numerical study of a novel counter-flow heat and mass exchanger for dew point evaporative cooling. Applied Thermal Engineering. 28 (2008) 1942-51.

[14] A.Y.T. Al-Zubaydi, G. Hong. Experimental study of a novel water-spraying configuration in indirect evaporative cooling. Applied Thermal Engineering. 151 (2019) 283-93.

[15] P. Xu, X. Ma, X. Zhao, K. Fancey. Experimental investigation of a super performance dew point air cooler. Applied Energy. 203 (2017).
[16] P. Xu, X. Ma, X. Zhao, K.S. Fancey. Experimental investigation on performance of fabrics for indirect evaporative cooling applications. Building and Environment. 110 (2016).
[17] Y. Liu, Y.G. Akhlaghi, X. Zhao, J. Li. Experimental and numerical investigation of a high-efficiency dew-point evaporative cooler. Energy & Buildings. 197 (2019).
[18] P.A. Doğramacı, D. Aydın. Comparative experimental investigation of novel organic materials for direct evaporative cooling applications in hot-dry climate. Journal of Building Engineering. 30 (2020).
[19] X. Zhao, S. Liu, S.B. Riffat. Comparative study of heat and mass exchanging materials for indirect evaporative cooling systems. Building and Environment. 43 (2007).
[20] Y. Wan, J. Lin, K.J. Chua, C. Ren. Similarity analysis and comparative study on the performance of counter-flow dew point evaporative coolers with experimental validation. Energy Conversion and Management. 169 (2018).
[21] Y. Min, Y. Chen, H. Yang. Numerical study on indirect evaporative coolers considering condensation: A thorough comparison between cross flow and counter flow. International Journal of Heat and Mass Transfer. 131 (2019).
[22] B. Zheng, C. Guo, T. Chen, Q. Shi, J. Lv, Y. You. Development of an experimental validated model of cross-flow indirect evaporative cooler with condensation. Applied Energy. 252 (2019).
[23] S.S. Baakeem, J. Orfi, A. Mohamad, S. Bawazeer. The possibility of using a novel dew point air cooling system (M-Cycle) for A/C application in Arab Gulf Countries. Building and Environment. 148 (2019).
[24] B. Riangvilaikul, S. Kumar. An experimental study of a novel dew point evaporative cooling system. Energy and Buildings. 42 (2010) 637-44.
[25] B. Riangvilaikul, S. Kumar. Numerical study of a novel dew point evaporative cooling system. Energy and Buildings. 42 (2010) 2241-50.
[26] Y. Yang, C. Ren, C. Yang, M. Tu, B. Luo, J. Fu. Energy and exergy performance comparison of conventional, dew point and new external-cooling indirect evaporative coolers. Energy Conversion and Management. 230 (2021).
[27] L. Chun, G. Gong, P. Peng, Y. Wan, K.J. Chua, X. Fang, et al. Research on thermodynamic performance of a novel building cooling system integrating dew point evaporative cooling, air-carrying energy radiant air conditioning and vacuum membrane-based dehumidification (DAV-cooling system). Energy Conversion and Management. 245 (2021).
[28] Y. Golizadeh Akhlaghi, A. Badiei, X. Zhao, K. Aslansefat, X. Xiao, S. Shittu, et al.

A constraint multi-objective evolutionary optimization of a state-of-the-art dew point cooler using digital twins. Energy Conversion and Management. 211 (2020).
[29] H. Jafarian, H. Sayyaadi, F. Torabi. Modeling and optimization of dew-point evaporative coolers based on a developed GMDH-type neural network. Energy Conversion and Management. 143 (2017) 49-65.
[30] J. Lin, R. Wang, C. Li, S. Wang, J. Long, K.J. Chua. Towards a thermodynamically favorable dew point evaporative cooler via optimization. Energy Conversion and Management. 203 (2020).
[31] S. Delfani, M. Karami. Transient simulation of solar desiccant/M-Cycle cooling systems in three different climatic conditions. Journal of Building Engineering. 29 (2020) 101152.
[32] D. Pandelidis, A. Cichoń, A. Pacak, P. Drąg, M. Drąg, W. Worek, et al. Water desalination through the dewpoint evaporative system. Energy Conversion and Management. 229 (2021).
[33] D. Pandelidis, S. Anisimov. Numerical analysis of the heat and mass transfer processes in selected M-Cycle heat exchangers for the dew point evaporative cooling. Energy Conversion and Management. 90 (2015) 62-83.
[34] A. Sohani, Y. Farasati, H. Sayyaadi. A systematic approach to find the best road map for enhancement of a power plant with dew point inlet air pre-cooling of the air compressor. Energy Conversion and Management. 150 (2017) 463-84.
[35] P. Bichkar, O. Dandgaval, P. Dalvi, R. Godase, T. Dey. Study of Shell and Tube Heat Exchanger with the Effect of Types of Baffles. Procedia Manufacturing. 20 (2018).
[36] V. R., S. B., V. A., K. P. Study on the heat transfer characteristics of AlO-CuO/Water hybrid nanofluids in a shell and rotating wavy tube heat exchanger. IOP Conference Series: Materials Science and Engineering. 1130 (2021).
[37] S. Trivendra, K.A. Manoj, G. Tarun. Performance Enhancement and Analysis of Shell and Tube Type Heat Exchanger. IOP Conference Series: Materials Science and Engineering. 1116 (2021).
[38] S.S. V., K. R., S.G. D. Experimental Investigation of Heat Transfer Enhancement of Shell and Tube Heat Exchanger Using SnO2-Water and Ag-Water Nanofluids. Journal of Thermal Science and Engineering Applications. 12 (2020).
[39] P.J.J.M.o.C. Roache. Computational fluid dynamics. 28 (1976).
[40] V. Gnielinski. Fundamentals of Heat And Mass Transfer. (2007).
[41] R. American Society of Heating, I. Air Conditioning Engineers. ASHRAE handbook of fundamentals. Ashrae Handbook of Fundamentals. (1972).
[42] M.C. Engineering. Thermophysical properties of humid air, models and background. (2005).
[43] L. Jie, B.D. Thuan, R. Wang, C.K. Jon. The counter-flow dew point evaporative

778 cooler: Analyzing its transient and steady-state behavior. Applied Thermal Engineering.
779 143 (2018) 34-47.
780 [44] F. Wang, X. Huang, H. Yang, C. Yi, T.J.A.T.E. Sun. Experimental research on a
781 novel porous ceramic tube type indirect evaporative cooler. 125 (2017).
782 [45] F.J.R. Martinez, E.V. Gomez, R.H. Martin, J.M. Gutierrez, F.V.J.E. Diez, Buildings.
783 Comparative study of two different evaporative systems: an indirect evaporative cooler
784 and a semi-indirect ceramic evaporative cooler. 36 (2004) 696-708.
785 [46] J. Lee, D.Y. Lee. Experimental study of a counter flow regenerative evaporative
786 cooler with finned channels. International Journal of Heat & Mass Transfer. 65 (2013)
787 173-9.
788